The Dynamics of Multi-Spike Solutions to the One-Dimensional Gierer-Meinhardt Model

David Iron [1], Michael J. Ward [2]

Abstract

The dynamical behavior of spike-type solutions to a simplified form of the Gierer-Meinhardt activator-inhibitor model in a one-dimensional domain is studied asymptotically and numerically in the limit of small activator diffusivity ε. In the limit $\varepsilon \to 0$, a quasi-equilibrium solution for the activator concentration that has n localized peaks, or spikes, is constructed asymptotically using the method of matched asymptotic expansions. For an initial condition of this form, a differential-algebraic system of equations describing the evolution of the spike locations is derived. The equilibrium solutions for this system are discussed. The spikes are shown to evolve on a slow time scale $\tau = \varepsilon^2 t$ towards a stable equilibrium, provided that the inhibitor diffusivity D is below some threshold, and that a certain stability criterion on the quasi-equilibrium solution is satisfied throughout the slow dynamics. If this stability condition is not satisfied initially or else is no longer satisfied at some later value of the slow time τ, the quasi-equilibrium profile becomes unstable on an fast $O(1)$ time scale. It is shown numerically that this $O(1)$ instability leads to a spike collapse event. The asymptotic theory is compared with corresponding full numerical results.

1 Introduction

Turing [20] showed how stable spatially complex patterns can develop from small perturbations of spatially homogeneous initial data for a coupled system of reaction-diffusion equations. He then proposed that localized peaks in the concentration of one of the species in the reaction could be responsible for the process of morphogenesis. Since then, there have been many reaction-diffusion models proposed for pattern formation, including the well-known activator-inhibitor model of Gierer and Meinhardt [6], referred to below as the GM model. In the limit of small activator diffusivity, this model can produce a pattern of localized peaks, or spikes, in the activator concentration. The GM model, and various extensions of it, have been used to model localization phenomena in developmental biology [7] and pattern formation on sea shells [10].

[1]Department of Mathematics, Univ. of British Columbia, Vancouver, Canada V6T 1Z2
[2]corresponding author: Department of Mathematics, Univ. of British Columbia, Vancouver, Canada V6T 1Z2

The non-dimensional simplified GM model in a one-dimensional spatial domain is given by

$$a_t = \varepsilon^2 a_{xx} - a + \frac{a^p}{h^q}\,, \qquad -1 < x < 1\,, \quad t > 0\,, \tag{1.1a}$$

$$0 = D h_{xx} - \mu h + \varepsilon^{-1}\frac{a^m}{h^s}\,, \qquad -1 < x < 1\,, \quad t > 0\,, \tag{1.1b}$$

$$a_x(\pm 1, t) = h_x(\pm 1, t) = 0\,. \tag{1.1c}$$

Here a, h, $\varepsilon \ll 1$, $D > 0$, and $\mu > 0$ represent the scaled activator concentration, inhibitor concentration, small activator diffusivity, inhibitor diffusivity, and constant inhibitor decay rate. The exponents (p, q, m, s) in (1.1) are assumed to satisfy

$$p > 1, \qquad q > 0, \qquad m > 0, \qquad s \geq 0, \qquad 0 < \frac{p-1}{q} < \frac{m}{s+1}\,. \tag{1.2}$$

The dimensional analysis leading to (1.1) is given in [9]. The simplification to the GM model that is made is that we neglect the time derivative of the inhibitor field. A mathematical survey of results for the GM model in both one and several spatial dimensions is given in [14] and [25].

There has been much recent work on analyzing the behavior of solutions to (1.1). The existence of symmetric spike-type equilibria for (1.1 was first proved in [19]. More recently, the method of matched asymptotic expansions has been used in [8] and [23] to construct symmetric and asymmetric equilibrium spike-type solutions for (1.1) in the limit $\varepsilon \to 0$. The stability properties of these solutions has also been analyzed in [8] and [23]. A rigorous framework to analyze the stability of equilibria for (1.1) is given in [26]. In contrast to these many results on the equilibrium problem, there have been only a few attempts to analyze the dynamics of spike-type patterns for (1.1). In particular, the dynamics of a one-spike solution for (1.1) was studied in [8]. The motion of a one-spike solution for the GM model in a two spatial dimensional domain has been analyzed in [3] and [22]. The dynamics of a one-spike solution for an extension of (1.1) that allows for the effect of precursor gradients was studied in [22].

With the mathematical framework for the existence and stability of spike-type solutions for (1.1) already established, our goal in this paper is to analyze the dynamics of spike-type solutions to (1.1) in the limit $\varepsilon \to 0$. In particular, in the limit $\varepsilon \to 0$ the method of matched asymptotic expansions is used to construct a quasi-equilibrium solution for the activator concentration that has n spikes. For an initial condition of this form, a formal asymptotic method, together with the Fredholm alternative, is used to derive a differential-algebraic (DAE) system of equations describing the evolution of the spike locations. This DAE system represents a projection of the full dynamics of (1.1) onto a finite dimensional dynamical system. This analysis shows that the spike locations evolve

on a slow time scale $\tau = \varepsilon^2 t$ towards a stable equilibrium, provided that the inhibitor diffusivity D is below some threshold, and that a certain stability criterion on the quasi-equilibrium solution is satisfied throughout the slow dynamics.

This stability criterion for the quasi-equilibrium solution plays a central role in the evolution of a pattern of spikes. We show that at some time during the slow evolution, the quasi-equilibrium solution can be become unstable on a fast $O(1)$ time scale. An asymptotic analysis, together with a spectral result of [24], is used to derive a stability threshold that determines the precise conditions for which the instability will be triggered. An important feature of this instability is that it can be triggered even for patterns where the spikes are widely spaced. Numerical examples show that this instability leads to the annihilation of one spike in the spike sequence. At the end of an $O(1)$ time interval marking the duration of the collapse process, the resulting quasi-equilibrium profile regains its stability with regards to the $O(1)$ eigenvalues. The remaining spikes then evolve slowly until, either, they reach a stable symmetric equilibrium solution or until another $O(1)$ instability is triggered at a later time, which leads to further collapse events. We examine this scenario carefully for profiles with two and three spikes. The asymptotic theory is compared with corresponding full numerical results from (1.1).

In recent years there has been much work in characterizing the dynamics of localized solutions to phase transition models in one spatial dimension, including the well-known fourth-order Cahn-Hilliard model (see the survey paper [21] and the references therein). Consider the Cahn-Hilliard equation on a finite interval defined under the natural boundary conditions associated with the usual free-energy functional. In contrast to the spike-type solutions for (1.1), the Cahn-Hilliard equation supports the existence of a collection of shock-type solutions, represented locally by heteroclinic orbits of the corresponding stationary problem.

There are many interesting differences between the motion of a pattern of internal layers for the Cahn-Hilliard equation and the motion of a collection of spikes for the GM model (1.1). The first difference is that in the limit of thin interface thickness, the motion of the internal layers for the Cahn-Hilliard equation is exponentially slow or metastable, rather than algebraically slow as for (1.1). The second difference is that for the Cahn-Hilliard problem there is no mechanism for the triggering of an $O(1)$ instability for a pattern with widely separated internal layers. Thus, the coarsening or interface collapse process is very different than for (1.1). Specifically, for the Cahn-Hilliard model, over an exponentially long time interval the internal layers will either collapse against one of the boundaries of the domain or they will collapse together in pairs. These collapse events continue until eventually a stable equilibrium with exactly one internal layer remains. Equilibrium solutions with more than one internal layer are unstable. In contrast, depending on the value of the inhibitor

diffusivity D, it is possible to have a stable spike-type solution for (1.1) with more than one spike.

Spike-type solutions also occur for other reaction-diffusion systems including the Gray-Scott model (cf. [17], [4], [5], [12], [13], [16]). This model has some similarities to the GM model. The stability of equilibrium spike solutions on an infinite line has been studied in [5] and [12]. The Gray-Scott model also exhibits a phenomenon known as pulse-splitting, whereby, under certain conditions, a solitary spike will first split into two spikes. Each of the resulting spikes can then undergo further splitting events. This spike-replication behavior has been studied by many authors, including [17], [4], [16] and [13]. This splitting behavior does not occur for (1.1) in the limit $\varepsilon \to 0$ and $D = O(1)$, which we consider.

The outline of the paper is as follows. In §2 we construct a quasi-equilibrium solution for (1.1) with n spikes. We also derive a DAE system characterizing the dynamics of the spike locations. In §3 we survey the results of [8] and [23] for the existence and stability of spike-type patterns for (1.1). These equilibrium spatial patterns can be characterized by the equilibria of the DAE system. In §4 we analyze the mechanism by which the n-spike quasi-equilibrium solution can become unstable on a fast $O(1)$ time scale. We show that, at a given value of the slow time variable τ, the n-spike profile will be stable if and only if the maximum eigenvalue of a certain matrix, which depends on D and on the spike locations at time τ, is below some threshold. In §5 we present numerical simulations of the asymptotic DAE system for patterns with two and three spikes. We illustrate this instability with a few examples. The asymptotic theory is compared favorably with full numerical results from (1.1).

2 The Dynamics of Quasi-Equilibrium Solutions

We derive a system of ordinary differential equations describing the dynamics of the spike locations for an n-spike quasi-equilibrium solution to (1.1). The spike locations x_i are assumed to satisfy $-1 < x_i < x_{i+1} < 1$ for $i = 1, .., n-1$. In [8] a one-spike solution was analyzed in detail and it was found that the spike evolves on a long time-scale $t = O(\varepsilon^{-2})$. Hence, we expect that $x_i = x_i(\tau)$, where $\tau = \varepsilon^2 t$.

In the inner region near each x_i, we introduce the new variables

$$y_i = \varepsilon^{-1}(x - x_i)\,, \quad h_i(y_i,\tau) = h(x_i + \varepsilon y_i, \varepsilon^{-2}\tau)\,, \quad a_i(y_i,\tau) = a(x_i + \varepsilon y_i, \varepsilon^{-2}\tau)\,, \quad \tau = \varepsilon^2 t\,. \tag{2.1}$$

We then expand

$$h_i(y_i,\tau) = h_{i0}(y_i,\tau) + \varepsilon h_{i1}(y_i,\tau) + \cdots\,, \qquad a_i(y_i,\tau) = a_{i0}(y_i) + \varepsilon a_{i1}(y_i,\tau) + \cdots\,. \tag{2.2}$$

Substituting (2.2) into (1.1a) and (1.1b), we get to leading order that

$$a_{i0}'' - a_{i0} + a_{i0}^p/h_{i0}^q = 0\,, \qquad -\infty < y_i < \infty\,, \tag{2.3a}$$

$$h_{i0}'' = 0\,. \tag{2.3b}$$

Here the primes indicate derivatives with respect to y_i. In order to match to the outer solution below, we need that h_{i0} is bounded and that $a_{i0} \to 0$ as $|y_i| \to \infty$. Thus, from (2.3b), we get that

$$h_{i0} = H_i(\tau)\,, \tag{2.4a}$$

for some unknown H_i. The solution to (2.3a) is

$$a_{i0}(y_i) = H_i^\gamma u_c(y_i)\,, \qquad \text{where} \qquad \gamma = q/(p-1)\,, \tag{2.4b}$$

and $u_c(y)$ satisfies

$$u_c'' - u_c + u_c^p = 0\,, \qquad -\infty < y < \infty\,, \tag{2.5a}$$

$$u_c \to 0 \quad \text{as} \quad |y| \to \infty\,; \qquad u_c'(0) = 0\,, \qquad u_c(0) > 0\,. \tag{2.5b}$$

In particular, when $p = 2$ we have

$$u_c(y) = \frac{3}{2}\mathrm{sech}^2\,(y/2)\,. \tag{2.5c}$$

The $O(\varepsilon)$ problems obtained from substituting (2.2) into (1.1a) and (1.1b) are

$$a_{i1}'' - a_{i1} + \frac{p a_{i0}^{p-1}}{h_{i0}^q} a_{i1} = \frac{q a_{i0}^p}{h_{i0}^{q+1}} h_{i1} - a_{i0}'\,\dot{x}_i\,, \tag{2.6a}$$

$$D h_{i1}'' = -\frac{a_{i0}^m}{h_{i0}^s}\,. \tag{2.6b}$$

Here $\dot{x}_i \equiv dx_i/d\tau$. Substituting (2.4) into (2.6), we get

$$L(a_{i1}) \equiv a_{i1}'' - a_{i1} + p u_c^{p-1} a_{i1} = q H_i^{\gamma-1} u_c^p h_{i1} - H_i^\gamma u_c'\,\dot{x}_i\,, \tag{2.7a}$$

$$D h_{i1}'' = -H_i^{\gamma m - s} u_c^m\,. \tag{2.7b}$$

Since $L(u_c') = 0$, and $u_c' \to 0$ exponentially as $|y| \to \infty$, the right-hand side of (2.7a) must satisfy the solvability condition that it be orthogonal to u_c'. In this way, we get

$$\dot{x}_i \int_{-\infty}^{\infty} \left[u_c'(y)\right]^2\, dy \sim \frac{q}{H_i} \int_{-\infty}^{\infty} u_c^p u_c' h_{i1}\, dy_i\,. \tag{2.8}$$

Integrating (2.8) by parts twice, and using the facts that h_{i1} and u_c are even functions, we obtain

$$\dot{x}_i \int_{-\infty}^{\infty} \left[u_c'(y)\right]^2 \, dy \sim -\frac{q}{2H_i(p+1)} \left(\int_{-\infty}^{\infty} [u_c(y)]^{p+1} \, dy \right) \left(\lim_{y_i \to +\infty} h_{i1}' + \lim_{y_i \to -\infty} h_{i1}' \right) , \tag{2.9}$$

for $i = 1, .., n$.

Now in the outer region, defined away from $O(\varepsilon)$ regions near each x_i, a is exponentially small and we expand

$$h(x) = h_0(x) + o(\varepsilon) \, . \tag{2.10}$$

Since $\varepsilon \ll 1$, and a is localized, the term $\varepsilon^{-1} a^m / h^s$ in (1.1b) in the outer region behaves like a linear combination of delta functions centered at x_i for $i = 1, .., n$. Substituting (2.4) and (2.10) into (1.1b), and letting $\varepsilon \to 0$, we find that h_0 satisfies

$$D h_{0xx} - \mu h_0 = -b_m \sum_{i=1}^{n} H_i^{\gamma m - s} \delta(x - x_i) \, , \qquad b_m \equiv \int_{-\infty}^{\infty} [u_c(y)]^m \, dy \, , \tag{2.11a}$$

$$h_{0x}(\pm 1) = 0 \, . \tag{2.11b}$$

The solution to (2.11) is

$$h_0(x) = b_m \sum_{i=1}^{n} H_i^{\gamma m - s} G(x; x_i) \, , \tag{2.12}$$

where $G(x; x_i)$ satisfies

$$D G_{xx} - \mu G = -\delta(x - x_i) \, , \qquad -1 < x < 1 \, , \tag{2.13a}$$

$$G_x(\pm 1; x_i) = 0 \, . \tag{2.13b}$$

To match with the inner solutions near each x_i, we require for $i = 1, .., n$ that

$$h_0(x_i) = H_i \, , \tag{2.14a}$$

$$\lim_{y_i \to \infty} h_{i1}' + \lim_{y_i \to -\infty} h_{i1}' = h_{0x}(x_{i+}) + h_{0x}(x_{i-}) \, . \tag{2.14b}$$

From (2.14a) and (2.12), we obtain a nonlinear algebraic system for H_i, $i = 1, .., n$.

The final step in the derivation is to calculate the integral f defined by

$$f \equiv \frac{\int_{-\infty}^{\infty} [u_c(y)]^{p+1} \, dy}{\int_{-\infty}^{\infty} [u_c'(y)]^2 \, dy} \, . \tag{2.15}$$

To do so, we first multiply (2.5a) by u_c. Upon integrating the resulting equation over the domain, we obtain

$$\int_{-\infty}^{\infty} u_c u_c'' \, dy - \int_{-\infty}^{\infty} u_c^2 \, dy + \int_{-\infty}^{\infty} u_c^{p+1} \, dy = 0 \,. \tag{2.16}$$

Upon integrating the first term in this equation by parts, we get

$$-1 = e - f \,, \qquad \text{where} \qquad e \equiv \frac{\int_{-\infty}^{\infty} [u_c(y)]^2 \, dy}{\int_{-\infty}^{\infty} [u_c'(y)]^2 \, dy} \,. \tag{2.17}$$

To obtain an additional equation, we multiply (2.5a) by u_c' and integrate over the domain to fix the constant of integration. We then integrate the resulting expression again to get

$$1 = e - \frac{2f}{p+1} \,. \tag{2.18}$$

Solving (2.17) and (2.18), we obtain

$$f = \frac{2(p+1)}{p-1} \,. \tag{2.19}$$

The dynamics of the n-spike pattern is obtained by substituting (2.14) and (2.19) into (2.9) and (2.12). The main result is summarized as follows (relabeling H_i by h_i in the notation below):

Proposition 2.1: *For $\varepsilon \ll 1$, the quasi-equilibrium solution for a and h is given by*

$$a(x,t) \sim a_c \equiv \sum_{j=1}^{n} h_j^{\gamma} u_c \left[\varepsilon^{-1} (x - x_j) \right] \,, \tag{2.20a}$$

$$h(x,t) \sim h_c \equiv b_m \sum_{j=1}^{n} h_j^{\gamma m - s} G(x; x_j) \,, \tag{2.20b}$$

where $h_i = h_i(\tau)$ and $x_i = x_i(\tau)$ satisfy the following differential-algebraic system for $i = 1, .., n$

$$h_i = b_m \sum_{j=1}^{n} h_j^{\gamma m - s} G(x_i; x_j) \,, \tag{2.21a}$$

$$\frac{dx_i}{d\tau} \sim -\frac{2q b_m}{p-1} h_i^{-1} \left(h_i^{\gamma m - s} \langle G_x \rangle_i + \sum_{\substack{j=1 \\ j \neq i}}^{n} h_j^{\gamma m - s} G_x(x_i; x_j) \right) \,. \tag{2.21b}$$

Here u_c satisfies (2.5), b_m is defined in (2.11a), $\tau = \varepsilon^2 t$, and $\langle G_x \rangle_i \equiv \left[G_x(x_{i+}; x_i) + G_x(x_{i-}; x_i) \right] / 2$.

The system (2.21) can also be written in matrix form as

$$\boldsymbol{h} = b_m \mathcal{G} \boldsymbol{h}^{\gamma m - s}\,, \qquad \frac{d\boldsymbol{x}}{d\tau} \sim -\frac{2q b_m}{p-1} \mathcal{H}^{-1} \mathcal{P} \boldsymbol{h}^{\gamma m - s}\,, \tag{2.22}$$

where $d\boldsymbol{x}/d\tau \equiv (\dot{x}_1, \ldots, \dot{x}_n)^t$. Here we have defined

$$\mathcal{G} \equiv \begin{pmatrix} G(x_1;x_1) & \cdots & G(x_1;x_n) \\ \vdots & \ddots & \vdots \\ G(x_n;x_1) & \cdots & G(x_n;x_n) \end{pmatrix}\,, \qquad \mathcal{H} \equiv \begin{pmatrix} h_1 & 0 & \cdots & 0 \\ 0 & \ddots & \cdots & 0 \\ \vdots & \vdots & \ddots & \vdots \\ 0 & 0 & \cdots & h_n \end{pmatrix}\,, \tag{2.23a}$$

and

$$\mathcal{P} \equiv \begin{pmatrix} \langle G_x(x_1;x_1)\rangle_0 & \cdots & G_x(x_1;x_n) \\ \vdots & \ddots & \vdots \\ G_x(x_n;x_1) & \cdots & \langle G_x(x_n;x_n)\rangle_n \end{pmatrix}\,, \qquad \boldsymbol{h} \equiv \begin{pmatrix} h_1 \\ \vdots \\ h_n \end{pmatrix}\,, \qquad \boldsymbol{h}^{\gamma m - s} \equiv \begin{pmatrix} h_1^{\gamma m - s} \\ \vdots \\ h_n^{\gamma m - s} \end{pmatrix}\,. \tag{2.23b}$$

Alternatively, we can write (2.22) in terms of certain tridiagonal matrices. In Appendix A, we show that

$$\mathcal{G} = \frac{\mathcal{B}^{-1}}{\sqrt{\mu D}}\,, \tag{2.24}$$

where $\mathcal{B}$ is the tridiagonal matrix

$$\mathcal{B} \equiv \begin{pmatrix} c_1 & d_1 & 0 & \cdots & 0 & 0 & 0 \\ d_1 & c_2 & \ddots & \ddots & \ddots & 0 & 0 \\ 0 & \ddots & \ddots & \ddots & \ddots & \ddots & 0 \\ \vdots & \ddots & \ddots & \ddots & \ddots & \ddots & \vdots \\ 0 & \ddots & \ddots & \ddots & \ddots & \ddots & 0 \\ 0 & 0 & \ddots & \ddots & \ddots & c_{n-1} & d_{n-1} \\ 0 & 0 & 0 & \cdots & 0 & d_{n-1} & c_n \end{pmatrix}\,, \tag{2.25a}$$

with matrix entries defined by

$$c_1 = \coth\left[\theta(x_2 - x_1)\right] + \tanh\left[\theta(1 + x_1)\right]\,; \quad c_n = \coth\left[\theta(x_n - x_{n-1})\right] + \tanh\left[\theta(1 - x_n)\right]\,, \tag{2.25b}$$

$$c_j = \coth\left[\theta(x_{j+1} - x_j)\right] + \coth\left[\theta(x_j - x_{j-1})\right]\,, \quad j = 2, .., n-1\,, \tag{2.25c}$$

$$d_j = -\mathrm{csch}\left[\theta(x_{j+1} - x_j)\right]\,, \quad j = 1, .., n-1\,. \tag{2.25d}$$

Here $\theta = \sqrt{\mu/D}$.

Next, we calculate the matrix product $\mathcal{P}\mathcal{B}$ using the procedure as outlined in Appendix A. We find that $\mathcal{P}\mathcal{B}$ is a tridiagonal matrix of the form

$$\mathcal{P}\mathcal{B} \equiv \frac{1}{2D}\mathcal{P}_b\,, \qquad \text{where} \qquad \mathcal{P}_b \equiv \begin{pmatrix} e_1 & f_1 & 0 & \cdots & 0 & 0 & 0 \\ -f_1 & e_2 & \ddots & \ddots & \ddots & 0 & 0 \\ 0 & \ddots & \ddots & \ddots & \ddots & \ddots & 0 \\ \vdots & \ddots & \ddots & \ddots & \ddots & \ddots & \vdots \\ 0 & \ddots & \ddots & \ddots & \ddots & \ddots & 0 \\ 0 & 0 & \ddots & \ddots & \ddots & e_{n-1} & f_{n-1} \\ 0 & 0 & 0 & \cdots & 0 & -f_{n-1} & e_n \end{pmatrix}. \tag{2.26a}$$

The matrix entries are defined by

$$e_1 = \tanh\left[\theta(1+x_1)\right] - \coth\left[\theta(x_2-x_1)\right]\,; \quad e_n = \coth\left[\theta(x_n-x_{n-1})\right] - \tanh\left[\theta(1-x_n)\right]\,, \tag{2.26b}$$

$$e_j = \coth\left[\theta(x_j-x_{j-1})\right] - \coth\left[\theta(x_{j+1}-x_j)\right]\,, \quad j = 2,..,n-1\,, \tag{2.26c}$$

$$f_j = \operatorname{csch}\left[\theta(x_{j+1}-x_j)\right]\,, \quad j = 1,..,n-1\,. \tag{2.26d}$$

Substituting (2.24) into (2.22), we obtain the following result equivalent to (2.21):

Corollary 2.1: *The differential-algebraic system (2.21) is equivalent to the matrix system*

$$\frac{d\boldsymbol{x}}{d\tau} \sim -\frac{q}{p-1}\sqrt{\frac{\mu}{D}}\mathcal{H}^{-1}\mathcal{P}_b\boldsymbol{h}\,, \qquad \mathcal{B}\boldsymbol{h} = \frac{b_m}{\sqrt{\mu D}}\boldsymbol{h}^{\gamma m-s}\,. \tag{2.27}$$

Here $\mathcal{H}$, $\mathcal{B}$ and $\mathcal{P}_b$ are given in (2.23a), (2.25), and (2.26), respectively.

The advantage of this formulation over (2.21) is that (2.27) is expressed only in terms of tridiagonal matrices. Starting with certain initial data $\boldsymbol{x}(0)$, in §5 we give numerical examples showing the evolution of the quasi-equilibrium solution (2.20) and (2.27) towards a stable equilibrium solution. These asymptotic results are also compared with full numerical results computed from (1.1).

3 Symmetric and Asymmetric Equilibria

From (2.27), the equilibrium values of $\boldsymbol{h}$ and $\boldsymbol{x}$ satisfy

$$\mathcal{B}\boldsymbol{h} = \frac{b_m}{\sqrt{\mu D}}\boldsymbol{h}^{\gamma m-s}\,, \qquad \mathcal{P}_b\boldsymbol{h} = 0\,. \tag{3.1}$$

In this section we recall some results obtained in [8] and [23] for the existence and stability of symmetric and asymmetric spike patterns for (1.1).

For the symmetric spike patterns where $h_j = H$ for $j = 1, .., n$, the x_j are located at the symmetry points

$$x_j = -1 + \frac{2j-1}{k}\,, \qquad j = 1, .., k\,. \tag{3.2}$$

In this case, it was shown in [8] that $2\tanh(\theta/n)$, with $\theta = \sqrt{\mu/D}$, is an eigenvalue of $\mathcal{B}$ with associated eigenvector $\boldsymbol{v} \equiv (1, 1, .., 1)^t$. In addition, $\mathcal{P}_b \boldsymbol{v} = 0$. Hence, from (3.1), the common spike value $h_j = H$ is

$$H^{\gamma m-(s+1)} = \frac{2\sqrt{\mu D}}{b_m} \tanh\left(\frac{\theta}{n}\right)\,. \tag{3.3}$$

The symmetric n-spike solution is obtained by substituting (3.2) and $h_j = H$ into (2.20).

In [23], *asymmetric* n-spike equilibrium patterns are constructed asymptotically. These patterns consist of $n_1 > 0$ small spikes of type A and $n_2 = n - n_1 > 0$ large spikes of type B arranged in any particular order from left to right across the interval $[-1, 1]$ as

$$\text{ABAAB....B}\,, \qquad n_1 \ - \ \text{A's}\,, \qquad n_2 \ - \ \text{B's.} \tag{3.4}$$

A plot of such a solution with five spikes in an ABBAB pattern is shown in Fig. 1. The following result for asymmetric equilibrium spike patterns is obtained in [23].

Proposition 3.1(**see [23]**): *Let $\varepsilon \to 0$ and $D < D_m$, for some critical value D_m. Then, there exists an asymmetric n-spike equilibrium solution to (1.1) of the form (2.20), where h_j satisfies*

$$h_j^{\gamma m-(s+1)} = \left(\frac{2\sqrt{\mu D}}{b_m}\right) \tanh\left(l_j\theta\right)\,, \qquad \theta = \sqrt{\mu/D}\,. \tag{3.5}$$

Here for each j, $l_j = l$ or $l_j = \tilde{l}$, where l and $\tilde{l}$, with $l \neq \tilde{l}$, are determined in terms of n_1, n_2 and $\sqrt{\mu/D}$ by the nonlinear system

$$n_1 l + n_2 \tilde{l} = 1\,, \qquad b\left[l\sqrt{\mu/D}\right] = b\left[\tilde{l}\sqrt{\mu/D}\right]\,, \tag{3.6a}$$

where

$$b(z) \equiv \frac{\tanh^r z}{\cosh z}\,, \qquad r \equiv \frac{1}{\gamma m - (s+1)}\,. \tag{3.6b}$$

The value $l_j = l$ must occur $n_1 > 0$ times, while $l_j = \tilde{l}$ must occur $n_2 = n - n_1 > 0$ times. The small and large spikes can be arranged in any sequence. Finally, the spike locations x_j are found from

$$x_1 = l_1 - 1\,, \qquad x_k = 1 - l_k\,, \qquad x_{j+1} = x_j + l_{j+1} + l_j\,, \quad j = 1, .., k-2\,. \tag{3.7}$$

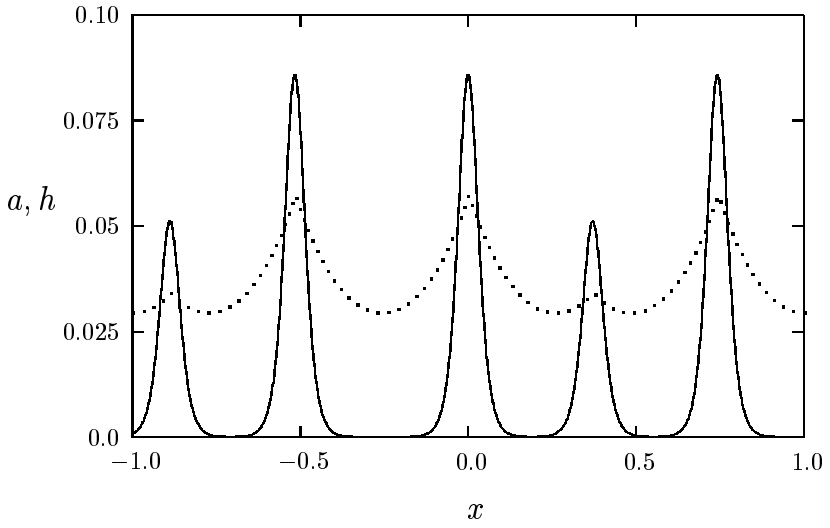

Figure 1: Plot of the activator and inhibitor concentration for a five-spike asymptotic asymmetric equilibrium solution with $\epsilon = .02$, $D = .04$, $\mu = 1$, and $(p, q, m, s) = (2, 1, 2, 0)$. The solid curve is the activator concentration and the dotted curve is the inhibitor concentration.

Detailed numerical computations determining the critical value D_m, as well as further more refined results for asymmetric equilibria, are obtained in [23]. For our purposes, the key point concerns the relationship between the symmetric and the asymmetric equilibrium spike patterns. Define an L_1-type norm of the equilibrium solution for a by

$$|a|_1 \equiv \sum_{j=1}^{n} h_j^{\gamma} \,. \tag{3.8}$$

The norm $|a|_1$ is a function of D. Label the symmetric branch with n spikes by s_n. Then, the following result was shown numerically in [23]:

Proposition 3.2(**see [23]**): *An n-spike asymmetric solution branch with n_1 small spikes of type A provides the connection, as D is varied, between the symmetric branches s_n and s_{n-n_1}. All of the asymmetric branches with n spikes bifurcate from the symmetric branch s_n at the critical value $D = D_b$ given by*

$$D_b = \frac{\mu}{n^2 \left[\log\left(\sqrt{r} + \sqrt{r+1}\right)\right]^2} \,. \tag{3.9}$$

Here r is defined in (3.6b).

A formal asymptotic analysis is used in [8] and [23] to study the stability properties of symmetric and asymmetric spike patterns, respectively. In the analyses of [8] and [23], there are two classes of eigenvalues that need to be considered. The first class are the large $O(1)$ eigenvalues, resulting from global spike interactions. They correspond to strong instabilities of small perturbations of the equilibrium solution on an $O(1)$ time-scale. This type of instability, referred to here as a profile instability, is not contained in the system (2.27). The second class of eigenvalues are the small $O(\varepsilon^2)$ eigenvalues that are associated with near translation invariance and slow dynamics near the equilibrium solutions. These small eigenvalues arise from the linearization of (2.27) about equilibrium values for $\boldsymbol{h}$ and $\boldsymbol{x}$. Thus, these eigenvalues are contained in the system (2.27). Critical ranges of D that ensure the stability of the equilibrium solution with respect to both classes of eigenvalues are derived in [8] and [23]. These critical values of D are obtained from studying the spectrum of certain matrix eigenvalue problems that result from a formal asymptotic analysis on the eigenvalue problem associated with the differential equation. A rigorous approach to derive these matrix eigenvalue problems from the associated differential equation is given in [26]. The original approach of [8], which relies heavily on the use of Green's function techniques, was motivated by the approach taken in [15] for studying the stability of pulse-type solutions in the Fitz-Hugh Nagumo equation.

The main qualitative stability conclusions from the analyses of [8] and [23] are as follows. For a certain nontrivial range of D near the bifurcation value D_b, each n-spike asymmetric solution branch that bifurcates from the symmetric branch s_n is stable with respect to the large $O(1)$ eigenvalues. However, based on numerical evidence, each of these bifurcating asymmetric branches is always unstable with respect to the small $O(\varepsilon^2)$ eigenvalues. The symmetric branch is stable with respect to the large eigenvalues when $D < D_n$ and is stable with respect to the small eigenvalues when $D < D_b$. Here D_n for $n \geq 2$, is given by

$$D_n = 4\mu n^{-2}\left[\ln\left(\beta + \sqrt{\beta^2 - 1}\right)\right]^{-2}, \qquad \beta \equiv 1 + (1 + \cos[\pi/k])\, r\,, \tag{3.10}$$

where r is defined in (3.6b). These two critical values of D satisfy the inequality $D_b < D_n$. As shown in [8], $n = 1$ is a special case and for this value D_1 is exponentially large as $\varepsilon \to 0$. In Fig. 2 we plot a bifurcation diagram of $|a|_1$ versus D, showing the asymmetric and symmetric branches with three or fewer spikes and their stability ranges with respect to the large $O(1)$ eigenvalues.

The implication of these results is that there are many equilibria of the quasi-equilibrium dynamics (2.27) with exactly n interior spikes. One of them corresponds to the symmetric spike pattern, and the rest correspond to asymmetric patterns. However, only the symmetric branches will be stable with respect to both the large and small eigenvalues when $D < D_b$. Hence, it is rea-

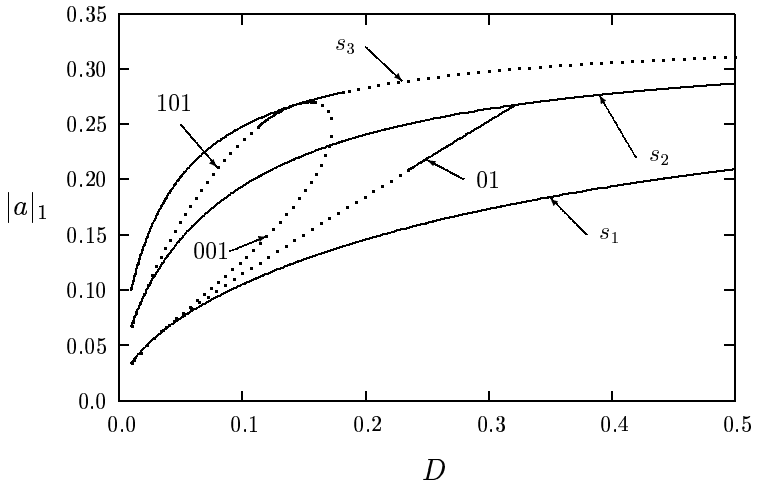

Figure 2: Plot of $|a|_1$ defined in (3.8) versus D for solutions with three or fewer spikes. Here $\mu = 1$ and $(p, q, m, s) = (2, 1, 2, 0)$. The symmetric branch with n spikes is labeled by s_n. The asymmetric patterns AB, BAB, and AAB are labeled by 01, 101, and 001, respectively. The portions of the branches that are solid (dotted) are stable (unstable) with respect to the large $O(1)$ eigenvalues.

sonable to expect that when $D < D_b$ the quasi-equilibrium dynamics (2.27) starting from certain initial $\boldsymbol{x}(0)$, will tend to a symmetric equilibrium with n spikes. Based on the numerical evidence of §5, a necessary condition for this to occur is that the quasi-equilibrium solution is stable with respect to the large $O(1)$ eigenvalues *throughout* the slow dynamics. For symmetric equilibria, this stability threshold is given by D_n in (3.10). For the quasi-equilibrium solution, the stability threshold depends on the values of $\boldsymbol{h}$ and $\boldsymbol{x}$ at a given τ.

4 Stability of the Profile: The Large Eigenvalues

We now examine the stability, at a fixed value of τ, of the quasi-equilibrium profile constructed in §2. The quasi-equilibrium profile of §2 varies on a slow time-scale $\tau = \varepsilon^2 t$. We would like to determine whether this profile can undergo an instability on a fast time-scale of $O(1)$. Hence, since there is a time-scale separation when $\varepsilon \ll 1$, in the eigenvalue analysis below we can treat τ as being a fixed parameter. To derive the eigenvalue problem, we substitute

$$a(x,t) = a_c + e^{\lambda t}\phi(x)\,, \qquad h(x,t) = h_c + e^{\lambda t}\eta(x)\,, \tag{4.1}$$

into (1.1) where a_c and h_c are defined in (2.20), and $\eta \ll 1$ and $\phi \ll 1$. This leads to

$$\varepsilon^2\phi_{xx} - \phi + \frac{pa_c^{p-1}}{h_c^q}\phi - \frac{qa_c^p}{h_c^{q+1}}\eta = \lambda\phi\,, \qquad -1 < x < 1\,, \tag{4.2a}$$

$$D\eta_{xx} - \mu\eta = -\varepsilon^{-1}m\frac{a_c^{m-1}}{h_c^s}\phi + \varepsilon^{-1}s\frac{a_c^m}{h_c^{s+1}}\eta\,, \qquad -1 < x < 1\,, \tag{4.2b}$$

$$\phi_x(\pm 1) = \eta_x(\pm 1) = 0\,. \tag{4.2c}$$

The spectrum of (4.2) contains large eigenvalues that are $O(1)$ as $\varepsilon \to 0$. Our analysis predicts that the quasi-equilibrium profile becomes unstable on an $O(1)$ time-scale when the $x_i(\tau)$, $h_i(\tau)$, for $i = 1, .., n$, are such that (4.2) has an eigenvalue with $\mathrm{Re}(\lambda) > 0$. This prediction is confirmed from the computational results in §5 of the full system (1.1)

We now proceed with the eigenvalue analysis. We look for an eigenfunction of (4.2) in the form

$$\phi(x) \sim \sum_{j=1}^{k} \phi_j\left[\varepsilon^{-1}(x - x_j)\right]\,, \tag{4.3}$$

where $\phi_j(y) \to 0$ exponentially as $|y| \to \infty$. Then, the right-hand side of (4.2b) with $s = 0$ behaves like a sum of delta functions when $\varepsilon \ll 1$. Substituting (2.20) and (4.3) into (4.2b), we get

$$D\eta_{xx} - \left[\mu + sb_m\sum_{j=1}^{n} h_j^{\gamma m-(s+1)}\delta(x - x_j)\right]\eta = -\sum_{j=1}^{n}\omega_j\delta(x - x_j)\,, \tag{4.4a}$$

$$\eta_x(\pm 1) = 0\,, \tag{4.4b}$$

where

$$\omega_j \equiv mh_j^{\gamma(m-1)-s}\int_{-\infty}^{\infty} u_c^{m-1}\phi_j\,dy\,. \tag{4.4c}$$

This problem is equivalent to

$$D\eta_{xx} - \mu\eta = 0\,, \qquad -1 < x < 1\,; \qquad \eta_x(\pm 1) = 0\,, \tag{4.5a}$$

$$[\eta]_j = 0\,, \qquad [D\eta_x]_j = -\omega_j + sb_m h_j^{\gamma m-(s+1)}\eta(x_j)\,, \tag{4.5b}$$

where $[v]_j \equiv v(x_{j+}) - v(x_{j-})$. By solving this system on each subinterval as in Appendix A, we can show that

$$\left(\mathcal{B} + \frac{sb_m}{\sqrt{\mu D}}\mathcal{H}^{\gamma m-(s+1)}\right)\boldsymbol{\eta} = \boldsymbol{\omega}/\sqrt{\mu D}\,, \qquad \boldsymbol{\eta} \equiv \begin{pmatrix} \eta(x_1) \\ \vdots \\ \eta(x_n) \end{pmatrix}\,, \qquad \boldsymbol{\omega} \equiv \begin{pmatrix} \omega_1 \\ \vdots \\ \omega_n \end{pmatrix}\,. \tag{4.6}$$

Here $\mathcal{H}$ and $\mathcal{B}$ are defined in (2.23a) and (2.25), respectively. Since $s > 0$ and $\mathcal{H}$ is a positive matrix, we can solve for $\boldsymbol{\eta}$ as

$$\boldsymbol{\eta} = \frac{mb_m}{\sqrt{\mu D}} \left(\mathcal{B} + \frac{sb_m}{\sqrt{\mu D}} \mathcal{H}^{\gamma m-(s+1)} \right)^{-1} \mathcal{H}^{\gamma(m-1)-s} \left(\frac{\int_{-\infty}^{\infty} u_c^{m-1} \boldsymbol{\phi}\, dy}{\int_{-\infty}^{\infty} u_c^m\, dy} \right) . \tag{4.7}$$

Next, we substitute (2.20) and (4.3) into (4.2a) to obtain, for $j = 1, .., n$, that

$$\phi_j'' - \phi_j + p u_c^{p-1} \phi_j - q h_j^{\gamma-1} u_c^p \eta(x_j) = \lambda \phi_j \,, \qquad -\infty < y < \infty \,, \tag{4.8}$$

with $\phi_j(y) \to 0$ as $y \to \infty$. We can write (4.8) in matrix form as

$$\boldsymbol{\phi}'' - \boldsymbol{\phi} + p u_c^{p-1} \boldsymbol{\phi} - q u_c^p \mathcal{H}^{\gamma-1} \boldsymbol{\eta} = \lambda \boldsymbol{\phi} \,. \tag{4.9}$$

Substituting (4.7) into (4.9), we obtain the eigenvalue problem

$$\boldsymbol{\phi}'' - \boldsymbol{\phi} + p u_c^{p-1} \boldsymbol{\phi} - mq u_c^p \left(\frac{\int_{-\infty}^{\infty} u_c^{m-1} \mathcal{E} \boldsymbol{\phi}\, dy}{\int_{-\infty}^{\infty} u_c^m\, dy} \right) = \lambda \boldsymbol{\phi} \,, \qquad -\infty < y < \infty \,, \tag{4.10a}$$

$$\boldsymbol{\phi} \to 0 \,, \quad \text{as} \quad |y| \to \infty \,, \tag{4.10b}$$

where the matrix $\mathcal{E}$ is defined by

$$\mathcal{E} \equiv \frac{b_m}{\sqrt{\mu D}} \mathcal{H}^{\gamma-1} \left(\mathcal{B} + \frac{sb_m}{\sqrt{\mu D}} \mathcal{H}^{\gamma m-(s+1)} \right)^{-1} \mathcal{H}^{\gamma m-(s+1)} \mathcal{H}^{1-\gamma} \,. \tag{4.11}$$

Since $\mathcal{G} = \mathcal{B}^{-1}/\sqrt{\mu D}$ is positive definite and $\mathcal{H}$ is a positive diagonal matrix, we conclude that $\mathcal{E}$ has real positive eigenvalues. We decompose $\mathcal{E}$ as

$$\mathcal{E} = \mathcal{S}^{-1} \Lambda_e \mathcal{S} \,, \tag{4.12}$$

for some nonsingular matrix $\mathcal{S}$. Then, upon defining $\boldsymbol{\psi} = \mathcal{S}\boldsymbol{\phi}$, we obtain from (4.10) that

$$\boldsymbol{\psi}'' - \boldsymbol{\psi} + p u_c^{p-1} \boldsymbol{\psi} - mq u_c^p \left(\frac{\int_{-\infty}^{\infty} u_c^{m-1} \Lambda_e \boldsymbol{\psi}\, dy}{\int_{-\infty}^{\infty} u_c^m\, dy} \right) = \lambda \boldsymbol{\psi} \,, \qquad -\infty < y < \infty \,, \tag{4.13a}$$

$$\boldsymbol{\psi} \to 0 \,, \quad \text{as} \quad |y| \to \infty \,. \tag{4.13b}$$

Since Λ_e is a diagonal matrix we obtain n uncoupled problems from (4.13).

The next step is to determine the conditions for which $\mathrm{Re}(\lambda) < 0$ in (4.13). For this we need the following key result of Wei [24]:

Theorem(**Wei [24]**): *Let $\beta > 0$ and consider the nonlocal eigenvalue problem for $\phi(y)$*

$$\phi'' - \phi + p u_c^{p-1}\phi - \beta(p-1)u_c^p \left(\frac{\int_{-\infty}^{\infty} u_c^{m-1}\phi\, dy}{\int_{-\infty}^{\infty} u_c^m dy} \right) = \lambda\phi\,, \qquad -\infty < y < \infty\,, \tag{4.14a}$$

$$\phi \to 0 \quad \text{as} \quad |y| \to \infty\,, \tag{4.14b}$$

corresponding to eigenpairs for which $\lambda \neq 0$. Here $u_c(y)$ satisfies (2.5). Let $\lambda_0 \neq 0$ be the eigenvalue of (4.14) with the largest real part. Then, if $\beta < 1$, we have

$$\mathrm{Re}(\lambda_0) > 0\,. \tag{4.15}$$

Alternatively, if $\beta > 1$ and if either of the following two conditions hold

$$\text{(i)} \quad m = 2\,,\ 1 < p \le 5\,, \qquad \text{or} \qquad \text{(ii)} \quad m = p+1\,,\ p > 1\,, \tag{4.16a}$$

then

$$\mathrm{Re}(\lambda_0) < 0\,. \tag{4.16b}$$

The proof of (4.16) is given in Lemma A and Theorem 1.4 of [24]. The simple proof of (4.15) is given in Appendix E of [8]. By comparing (4.13) with (4.14), we obtain the following result on the spectrum of (4.13):

Proposition 4.1: *Let $\lambda_0 \neq 0$ be the eigenvalue of (4.13) with the largest real part and assume condition (4.16a) holds. Let α_1 be the minimum eigenvalue of the matrix $\mathcal{E}$ defined in (4.11). Then, Re$(\lambda_0) > 0$ when*

$$\alpha_1 < \frac{(p-1)}{qm}\,. \tag{4.17}$$

Also, Re$(\lambda_0) < 0$ when $\alpha_1 > (p-1)/qm$.

A more convenient criterion is obtained by writing $\mathcal{E}$ in (4.11) as $\mathcal{E} = \mathcal{H}^{\gamma-1}\left(\tilde{\mathcal{E}} + sI\right)^{-1}\mathcal{H}^{1-\gamma}$, where

$$\tilde{\mathcal{E}} \equiv \frac{\sqrt{\mu D}}{b_m}\mathcal{H}^{-\gamma m+(s+1)}\mathcal{B}\,. \tag{4.18}$$

The eigenvalues of $\mathcal{E}$ and $\left(\tilde{\mathcal{E}} + sI\right)^{-1}$ are identical. We can then rewrite Proposition 4.1 as the following simple criterion:

Corollary 4.1: *Let $\lambda_0 \neq 0$ be the eigenvalue of (4.13) with the largest real part and assume condition (4.16a) holds. Let e_m be the maximum eigenvalue of the tridiagonal matrix $\tilde{\mathcal{E}}$ defined in (4.18). Then, Re$(\lambda_0) > 0$ when*

$$e_m > \frac{qm}{(p-1)} - s\,. \tag{4.19}$$

Also, $Re(\lambda_0) < 0$ when $e_m < qm/(p-1) - s$.

The results of [8] and [23] for the stability of symmetric and asymmetric equilibrium spike patterns with respect to the large $O(1)$ eigenvalues were obtained from a criterion such as Corollary 4.1. In our numerical examples in §5 of the evolution of the quasi-equilibrium solution, we track the maximum eigenvalue of $\tilde{\mathcal{E}}$ as a function of τ and determine the behavior of the solution if the threshold in (4.19) is exceeded.

5 Comparison of Asymptotic and Numerical Results

We now compare the asymptotic results for the spike motion with corresponding numerical results computed from (1.1). Unless otherwise stated, in the comparisons below we have taken the parameter values $\mu = 1$, the exponent set $(p, q, m, s) = (2, 1, 2, 0)$, and $\varepsilon = 0.02$. The comparisons are made for various values of the inhibitor diffusivity D, of the number of spikes n, and of the initial spike locations $x_j(0)$, for $j = 1, .., n$. The time variable given in the plots below correspond to the slow time variable τ defined in (2.1) by $\tau = \varepsilon^2 t$. With $\varepsilon = .02$, we get $t = 2500\tau$.

To compute the full numerical results from (1.1), we use the NAG library code [11] with 2001 equidistant meshpoints. For given values of D, n, and $x_j(0)$ for $j = 1, .., n$, we take the quasi-equilibrium solution (2.20) to be the initial condition for a and h. To compute $a(x, 0)$ and $h(x, 0)$, we must determine the initial values $h_j(0)$, for $j = 1, .., n$, from the nonlinear algebraic system for h_j in (2.27). This is done using Newton's method. In the Newton iteration we require an initial guess for the h_j. This is quite a nontrivial task, and to do so we use one of the two different methods. The first method is to perform a homotopy in the spike locations starting from the symmetric equilibrium solution (3.2) and (3.3). The second method is a homotopy in the value of D, starting from a value of D where $D \gg 1$. When $D \gg 1$, we can use an initial guess of the form $h_j \approx h_\infty$, where the constant h_∞ is independent of j and is readily determined. From this starting point, the homotopy involves decreasing the value of D to the desired value. Sometimes one of these homotopy approaches failed. This failure, which is a result of the non-invertibility of the linearized system for the h_j at certain specific parameter values, is explained below. Once the nonlinear system for the h_j in (2.27) is solved, the initial condition for $a(x, 0)$ and $h(x, 0)$ is known from (2.20) and the NAG solver [11] is used to compute the solution to (1.1) at later times τ. The locations of the spikes from these numerical results were obtained by a local quadratic interpolation.

The asymptotic results were obtained by solving the differential-algebraic system (2.27) for $x_j(\tau)$ and $h_j(\tau)$ using the ODE solver [18] coupled together with Newton's method to determine

the h_j. Another method, which we found to work equally well, is to use the differential-algebraic solver DDASSL [2] directly. The initial values for $h_j(0)$ were obtained using one of the homotopy methods described above. It is very important to calculate the maximum eigenvalue e_m of (4.18) as a function of τ. The curve $e_m = e_m(\tau)$ is computed at each step by using the eigenvalue solver [1]. The asymptotic theory predicts that if $e_m > 2$ at any value of τ, the quasi-equilibrium profile develops an instability on an $O(1)$ time scale. This asymptotic prediction is verified below from numerical results obtained from the full numerical solution to (1.1).

In §5.1 and §5.2 we give asymptotic and numerical results for the case of $n = 2$ and $n = 3$, respectively. Some observations and a conjecture concerning the collapse process are discussed briefly in §5.3.

5.1 Two Spikes $n = 2$

When $n = 2$, the nonlinear system in (2.27) for h_j reduces to

$$c_1 h_1 + d_1 h_2 = b_m h_1^{\gamma m - s}/\sqrt{\mu D}\,, \tag{5.1a}$$

$$d_1 h_1 + c_2 h_2 = b_m h_2^{\gamma m - s}/\sqrt{\mu D}\,, \tag{5.1b}$$

where c_j and d_j are defined in (2.25a). From (5.1) we readily obtain an equation for h_1/h_2. The differential equations for x_j in (2.27) depend only on the ratio h_1/h_2. In this way, we obtain the next result.

Corollary 5.1: *When $n = 2$, the differential-algebraic system (2.27) is equivalent to*

$$\dot{x}_1 = -\zeta\left(\tanh[\theta(1+x_1)] - \coth[\theta(x_2-x_1)] + \operatorname{csch}[\theta(x_2-x_1)]/\xi\right)\,, \tag{5.2a}$$

$$\dot{x}_2 = -\zeta\left(-\xi\operatorname{csch}[\theta(x_2-x_1)] + \coth[\theta(x_2-x_1)] - \tanh[\theta(1-x_2)]\right)\,, \tag{5.2b}$$

where $\xi \equiv h_1/h_2$ satisfies

$$f(\xi) \equiv \operatorname{csch}[\theta(x_2-x_1)]\left(\xi^{\gamma m-s+1}-1\right) + \coth[\theta(x_2-x_1)]\left(\xi - \xi^{\gamma m-s}\right) + \tanh[\theta(1+x_1)]\xi - \tanh[\theta(1-x_2)]\xi^{\gamma m-s} = 0\,. \tag{5.2c}$$

Here $\zeta = q\theta/(p-1)$, where $\theta = \sqrt{\mu/D}$.

In the special case of symmetric initial data where $x_1(0) = -x_2(0)$, we have that $\xi \equiv 1$ is a root to (5.2c). In this symmetric case, $\xi = 1$ and $x_1(\tau) = -x_2(\tau)$ for all τ. Combining (5.2a) and (5.2b) we obtain the next result.

Corollary 5.2: *Let $n = 2$ and assume that the initial data is symmetric in the sense that $x_1(0) = -x_2(0)$. Let $y = x_2 - x_1$. Then, (5.2) is equivalent to the single differential equation*

$$\dot{y} = 2\zeta \left(\operatorname{csch}(\theta y) - \coth(\theta y) + \tanh\left[\theta\left(1 - y/2\right)\right]\right) , \tag{5.3}$$

where $\zeta = q\theta/(p-1)$ and $\theta = \sqrt{\mu/D}$.

The behavior of the spike dynamics depends on the value of D with respect to D_b, the initial positions of the spikes, and the initial value of the maximum eigenvalue e_m of Corollary 4.1 at $\tau = 0$. Recall from §3 and (3.9) that a two-spike symmetric equilibrium solution with spikes located at $x_1 = -x_2 = -1/2$ will be stable if $D < D_b \approx 0.3218$. We now gives some examples of the theory.

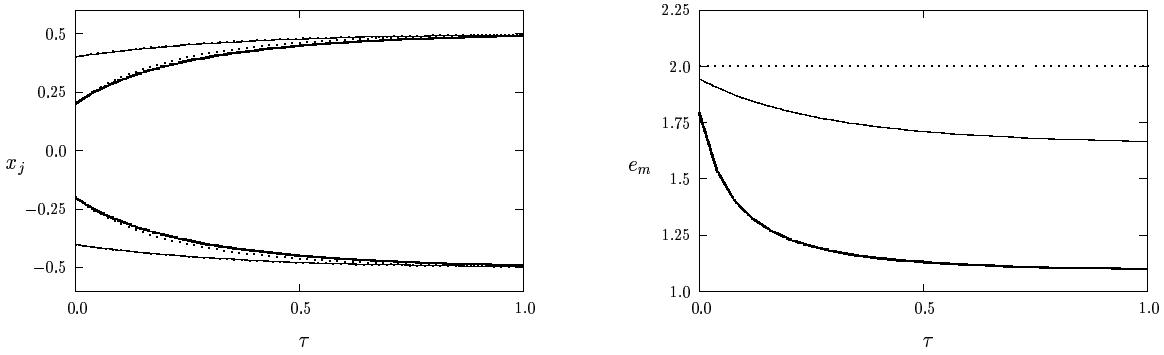

(a) x_j versus τ (b) e_m versus τ

Figure 3: In Fig. 3(a) we plot x_j versus τ for the two symmetric parameter sets in Example 1. The solid and heavy solid curves correspond to the full numerical results for Example 1a and Example 1b, respectively, given in (5.4). The asymptotic results computed from (5.3) correspond to the dotted curves. In Fig. 3(b) we plot the maximum eigenvalue e_m of (4.18) versus τ. In this figure the solid and heavy solid curves refer to Example 1a and Example 1b.

Example 1: (Symmetric Initial Data) We consider two different examples of symmetric initial data with $x_1(0) = -x_2(0)$. The parameter values are

$$\text{Example 1a:} \qquad x_1(0) = -0.4 = -x_2(0)\,, \qquad D = 0.4\,, \tag{5.4a}$$

$$\text{Example 1b:} \qquad x_1(0) = -0.2 = -x_2(0)\,, \qquad D = 0.1\,, \tag{5.4b}$$

Note that a symmetric equilibrium solution with two spikes is such that $x_1 = -x_2 = -1/2$.

At $\tau = 0$ we then compute the eigenvalue e_m from Corollary 4.1 that determines the stability of the initial quasi-equilibrium profile. For Examples 1a and 1b we compute numerically that $e_m(0) = 1.944$ and $e_m(0) = 1.793$, respectively. Thus, for both examples, the initial profile is stable with respect to the large $O(1)$ eigenvalues. However, in Example 1a we have $D > D_b$, whereas in Example 1b we have $D < D_b$. Therefore, it is only for Example 1b that the symmetric equilibrium solution is stable with respect to the small eigenvalues.

The asymptotic result for these two examples is obtained by integrating (5.3). A simple analysis shows that for any initial data $y(0) > 0$ and *any value* of D, the solution to the ODE (5.3) has the limiting asymptotic behavior $y \to 1$ as $\tau \to \infty$. Hence, this ODE predicts that $x_1 \to -1/2$ and $x_2 \to 1/2$ as $\tau \to \infty$ for Example 1a and for Example 1b.

To attempt to resolve this paradox, we refer to Proposition 11 of [8] where it was shown that when $D > D_b$ there is exactly one positive and one negative small eigenvalue for the linearization of (1.1) about the two-spike symmetric equilibrium solution. The positive eigenvalue becomes negative when D crosses below D_b. Thus, when $D > D_b$, the symmetric equilibrium corresponds to a saddle point in phase-space with one only stable direction towards the equilibrium. We conjecture that by taking symmetric initial data we approach the symmetric equilibrium solution along the stable manifold. Although an analytical verification of this conjecture requires is very difficult since it requires a global construction of the stable manifold, we can readily obtain some partial evidence consistent with our conjecture. The first observation, obtained from the analysis leading up to Proposition 11 of [8], is that in a small neighborhood of the symmetric equilibrium solution the eigenfunction associated with the stable direction is the one for which the spikes have equal height. Secondly, we show in Example 4 below that when $D > D_b$ and the initial data is only slightly asymmetric, the time-dependent solution does not tend to a symmetric equilibrium solution.

τ	x_1 (num)	x_2 (num)	x_1 (asy)	x_2 (asy)
0.06	-0.4163	0.4163	-0.4157	0.4157
0.09	-0.4238	0.4238	-0.4225	0.4225
0.18	-0.4419	0.4419	-0.4399	0.4399
0.27	-0.4557	0.4557	-0.4535	0.4535
0.36	-0.4662	0.4662	-0.4639	0.4639
0.45	-0.4742	0.4742	-0.4721	0.4721
0.54	-0.4803	0.4803	-0.4783	0.4783
0.63	-0.4850	0.4850	-0.4832	0.4832

Table 1: The numerical and asymptotic results for x_1 and x_2 versus τ for Example 1a.

τ	x_1 (num)	x_2 (num)	x_1 (asy)	x_2 (asy)
0.06	-0.2762	0.2762	-0.2670	0.2670
0.12	-0.3283	0.3283	-0.3146	0.3146
0.24	-0.3946	0.3946	-0.3779	0.3779
0.36	-0.4337	0.4337	-0.4177	0.4177
0.42	-0.4472	0.4472	-0.4321	0.4321
0.48	-0.4579	0.4579	-0.4439	0.4439
0.66	-0.4786	0.4786	-0.4681	0.4681
0.78	-0.4863	0.4863	-0.4781	0.4781

Table 2: The numerical and asymptotic results for x_1 and x_2 versus τ for Example 1b.

For Examples 1a and 1b, in Fig. 3(a) we compare the trajectories $x_j(\tau)$ for $j = 1, 2$ computed from the asymptotic result (5.3) with the full numerical results computed from (1.1). Selected values for x_j from the asymptotic and full numerical results are shown in Table 1 and Table 2 for Examples 1a and 1b, respectively. The agreement is found to be close. In Fig. 3(b) we plot $e_m = e_m(\tau)$ for both examples. The threshold for an $O(1)$ instability is given by the dotted line in Fig. 3(b). Notice that e_m decreases as τ increases, so that no $O(1)$ instability occurs at later times. In Fig. 4(a) and Fig. 4(b) we plot the numerical solution a versus x at different values of τ for Example 1a and Example 1b, respectively.

Example 2: (Generic Initial Data) We consider two sets of generic initial data. The parameter values are taken to be

$$\text{Example 2a:} \qquad x_1(0) = -0.2\,, \quad x_2(0) = 0.32\,, \qquad D = 0.1\,, \tag{5.5a}$$

$$\text{Example 2b:} \qquad x_1(0) = -0.8\,, \quad x_2(0) = 0.20\,, \qquad D = 0.2\,. \tag{5.5b}$$

For Examples 2a and 2b we compute numerically from (4.18) that the maximum eigenvalue e_m in Corollary 4.1 at $\tau = 0$ is $e_m(0) = 1.4846$ and $e_m(0) = 1.4106$, respectively. Thus, for both examples, the initial profile is stable with respect to the large $O(1)$ eigenvalues. For both examples $D < D_b$ so that the symmetric equilibrium solution is stable.

For Examples 2a and 2b, in Fig. 5(a) we compare the trajectories $x_j(\tau)$ for $j = 1, 2$ computed from the asymptotic result (5.2) with the full numerical results computed from (1.1). Selected values for x_j from the asymptotic and full numerical results are shown in Table 3 and Table 4 for Examples 2a and 2b, respectively. As seen in Fig. 5(b) the maximum eigenvalue once again decreases as τ increases and so no $O(1)$ instability is triggered at later times. In Fig. 6(a) and

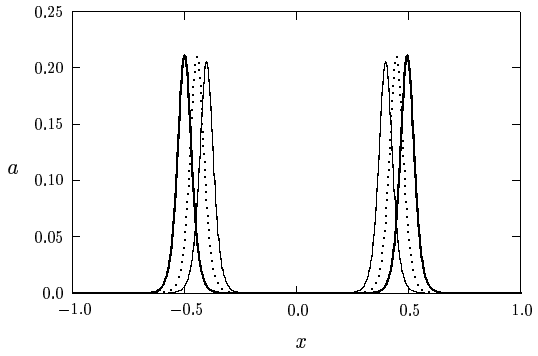

(a) a versus x at different τ (Example 1a)

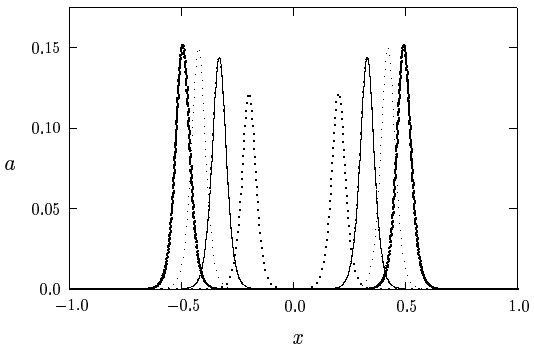

(b) a versus x at different τ (Example 1b)

Figure 4: The numerical results for a versus x at different values of τ are plotted in Fig. 4(a) for Example 1a and in Fig. 4(b) for Example 1b. In Fig. 4(a) the solid, dotted, and heavy solid curves correspond to $\tau = 0.0$, $\tau = .202$, and $\tau = 1.202$, respectively. In Fig. 4(b) the dotted, solid, light dotted, and heavy solid curves correspond to $\tau = 0.0$, $\tau = .123$, $\tau = .321$, and $\tau = 1.002$, respectively.

Fig. 6(b) we plot the numerical solution for the activator concentration a versus x at different values of τ for Example 2a and Example 2b, respectively.

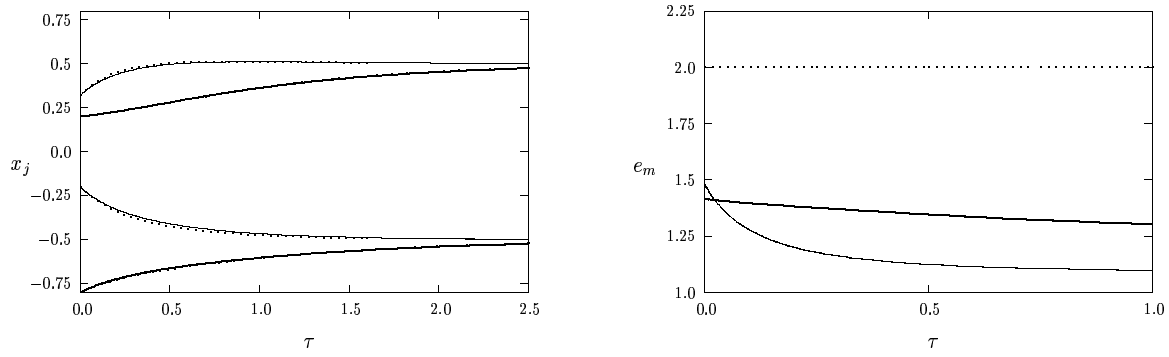

(a) x_j versus τ (b) e_m versus τ

Figure 5: In Fig. 5(a) we plot x_j versus τ for the two parameter sets in Example 2. The solid and heavy solid curves correspond to the full numerical results for Example 2a and Example 2b, respectively, given in (5.5). The asymptotic results computed from (5.2) correspond to the dotted curves. In Fig. 5(b) we plot the maximum eigenvalue e_m of (4.18) versus τ. The solid and heavy solid curves refer to Example 2a and Example 2b.

Example 3: (An Initial $O(1)$ Instability) We take the parameter values

$$x_1(0) = -0.2\,, \quad x_2(0) = 0.32\,, \qquad D = 0.25\,. \tag{5.6}$$

In this case, we compute numerically from (4.18) that $e_m(0) = 2.228$. Thus, the initial profile is unstable with respect to the large positive eigenvalues. Since $e_m(0) > 0$, the asymptotic result (5.2) does not apply.

In Fig. 7(a) we plot the numerically computed activator concentration a versus x for $\tau = 0$ and for several very small values of τ. In terms of t, the plots in Fig. 7(a) are for $t < 20.0$. What we observe is that the smaller of the two initial spikes starts collapsing but that the spike locations remain quite fixed during the collapse. The other spike grows during the collapse of its neighbor. After the smaller spike has completely collapsed, the other one moves very slowly towards the symmetric one-spike equilibrium solution centered at the origin. This is shown in Fig. 7(b).

Example 4: (An $O(1)$ Instability at a Later Time) Next, we consider a case with near

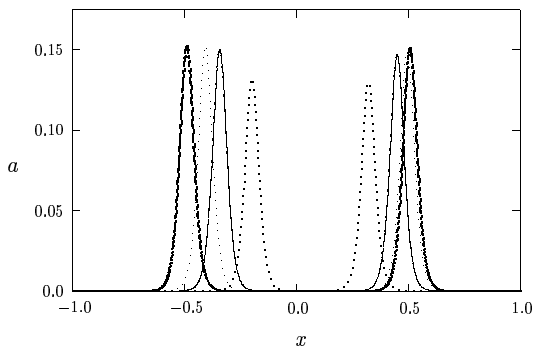

(a) a versus x at different τ (Example 2a)

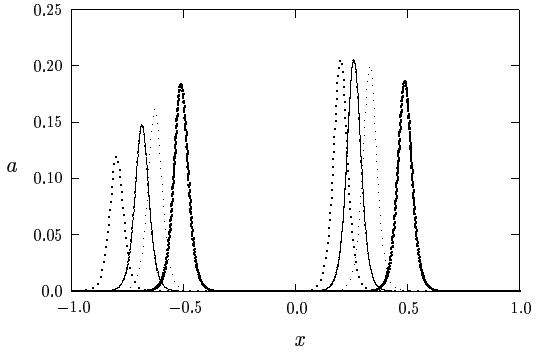

(b) a versus x at different τ (Example 2b)

Figure 6: The numerical results for a versus x at different values of τ are plotted in Fig. 6(a) for Example 2a and in Fig. 6(b) for Example 2b. In Fig. 6(a) the dotted, solid, light dotted, and heavy solid curves correspond to $\tau = 0.0$, $\tau = .202$, $\tau = .403$, and $\tau = 1.402$, respectively. In Fig. 6(b) the dotted, solid, light dotted, and heavy solid curves correspond to $\tau = 0.0$, $\tau = .404$, $\tau = .804$, and $\tau = 3.200$, respectively.

τ	x_1 (num)	x_2 (num)	x_1 (asy)	x_2 (asy)
0.032	-0.2329	0.3526	-0.2284	0.3480
0.08	-0.2724	0.3906	-0.2634	0.3817
0.30	-0.3782	0.4789	-0.3622	0.4667
0.40	-0.4051	0.4954	-0.3892	0.4853
0.48	-0.4218	0.5036	-0.4063	0.4953
0.60	-0.4410	0.5104	-0.4265	0.5048
0.80	-0.4619	0.5138	-0.4500	0.5118
1.28	-0.4856	0.5100	-0.4788	0.5117

Table 3: The numerical and asymptotic results for x_1 and x_2 versus τ for Example 2a.

τ	x_1 (num)	x_2 (num)	x_1 (asy)	x_2 (asy)
0.06	-0.6556	0.2161	-0.6528	0.2157
0.66	-0.6171	0.3400	-0.6136	0.3383
0.84	-0.6003	0.3678	-0.5981	0.3657
1.00	-0.5866	0.3891	-0.5854	0.3868
1.40	-0.5585	0.4299	-0.5589	0.4273
1.60	-0.5476	0.4445	-0.5485	0.4420
1.90	-0.5347	0.4611	-0.5359	0.4588
2.50	-0.5180	0.4808	-0.5192	0.4793

Table 4: The numerical and asymptotic results for x_1 and x_2 versus τ for Example 2b.

symmetric initial data. We take

$$x_1(0) = -0.4\,, \qquad x_2(0) = .401\,, \qquad D = 0.4\,. \tag{5.7}$$

In this case, we compute from (4.18) that $e_m(0) = 1.941$, so that the initial quasi-equilibrium profile is stable with respect to the large eigenvalues. However, in this example, the quasi-equilibrium profile will become unstable with respect to the large eigenvalues as time increases. This instability will trigger a spike collapse event.

The results from these computations are plotted in Figures 8(a) and 8(b). Initially, the numerical results from the full system and the asymptotic system agree. However, at a later time these results start to diverge and one of the spikes from the numerical computation becomes unstable before the predicted asymptotic time. We speculate that the reason for this is that the nearly symmetric data is initially very close to the stable manifold of a two-spike solution and, thus, remains close to the

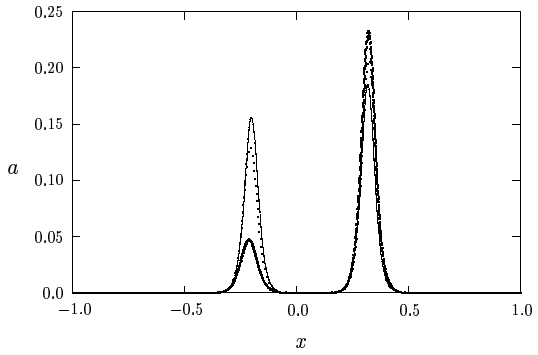

(a) a versus x (collapse event)

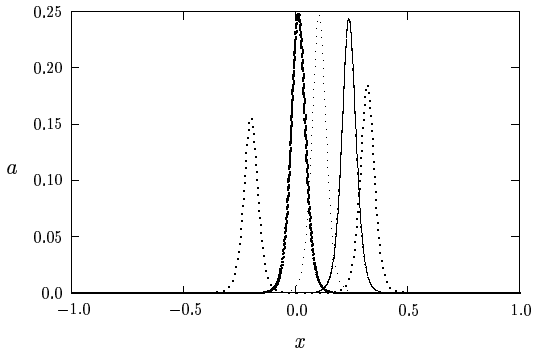

(b) a versus x (one-spike motion)

Figure 7: The numerical results for a versus x at different values of τ are plotted for Example 3. In Fig. 7(a), where we show the collapse event, the solid, dotted, and heavy solid curves correspond to $\tau = 0.0$, $\tau = 0.00504$, and $\tau = 0.00704$, respectively. In Fig. 7(b), where one spike drifts towards the origin, the solid, light dotted, and heavy solid curves correspond to $\tau = 0.4$, $\tau = 1.6$, and $\tau = 4.8$, respectively. The initial condition at $\tau = 0$ is the dotted curve.

stable manifold for some time. However, as the solution diverges away from the stable manifold, small numerics errors in the simulation as well as small differences between the results from the asymptotic and full system begin to grow rapidly. We conjecture that it is this growth in errors that is responsible for the discrepancies between the simulation of the full system and that of the asymptotic differential equations.

5.2 Three Spikes $n = 3$

We now consider some examples with three initial spikes. From §3 and (3.9) it follows that a three-spike symmetric equilibrium solution with spikes located at $x_2 = 0$ and $x_3 = -x_1 = 2/3$ will be stable if $D < D_b \approx 0.1430$. We now gives two examples of the theory.

Example 5: (Symmetric Initial Data) We first consider the case of three spikes with symmetric initial data (i.e. $x_1(0) = -x_3(0)$ and $x_2(0) = 0$). In this case the two outer spikes will have the same height, but the middle spike will generally have a different height. Thus, unlike the case of two spikes with symmetric initial data, we can not reduce the differential algebraic system (2.27 to a single ordinary differential equation.

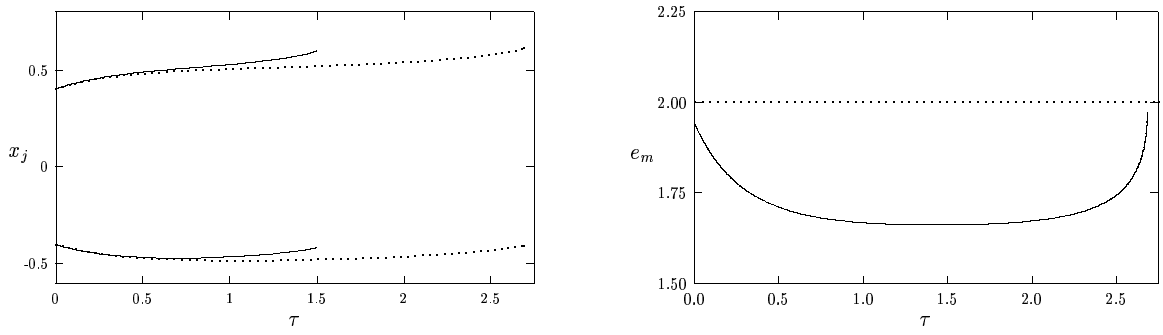

(a) x_j versus τ (b) e_m versus τ

Figure 8: In Fig. 8(a) we plot x_j versus τ for Example 4. The solid curve corresponds to the full numerical results and the dotted curves corresponds to the asymptotic results. In Fig. 8(b), we plot the maximum eigenvalue e_m of (4.18) versus τ.

Another important difference between the case of two and three spikes with symmetric initial data is in the form of the stable and unstable manifolds with respect to the small eigenvalues associated with a linearization around a three-spike symmetric equilibrium solution. For a two-spike solution both the stable and unstable manifolds are one-dimensional. However, in the case of three spikes, the linearization of (1.1) about a three-spike symmetric equilibrium solution shows that locally we have a one-dimensional stable manifold and a two-dimensional unstable manifold (cf. [8]). This stable manifold corresponds to spikes of equal height (cf. [8]). Thus, in this case, since a symmetric three-spike solution satisfying $x_1(0) = -x_3(0)$ and $x_2(0) = 0$ will not in general have spikes of equal height, it appears that these symmetric solutions are not confined to the stable manifold.

As an example, we take the parameter values

$$x_1(0) = -0.5\,, \quad x_2(0) = 0\,, \quad x_3(0) = 0.5\,, \quad D = 0.01\,. \tag{5.8}$$

For this example we calculate from (4.18) that $e_m(0) = 1.025$. Thus, the initial profile is stable with respect to the large $O(1)$ eigenvalues. The results of the simulations are shown in Fig. 9, and the numerical and asymptotic results for x_j are compared in Table 6. In this case e_m decreases as τ increases. Thus, no $O(1)$ instability is triggered and the spikes tend to their equilibrium locations.

τ	x_1 (num)	x_2 (num)	x_1 (asy)	x_2 (asy)
0.004	-0.40126	0.40226	$-.40762$	0.42297
0.032	-0.40894	0.41053	$-.40618$	0.42048
0.052	-0.41390	0.41614	$-.40971$	0.42662
0.08	-0.42032	0.42351	$-.41423$	0.43476
0.1	-0.42455	0.42844	$-.41717$	0.44026
0.3	-0.45404	0.46566	$-.43574$	0.48466
0.6	-0.47031	0.49756	$-.43768$	0.53190
0.988	-0.46514	0.52649	$-.40640$	0.59999

Table 5: The numerical and asymptotic results for x_1 and x_2 versus τ for Example 4.

Alternatively, if we take $D = 0.15$ and the same initial locations for the spikes as given in (5.8), then $e_m(0) = 2.6236$. This implies that the initial quasi-equilibrium solution is unstable. In this case, an $O(1)$ instability is triggered at $t = 0$, and similar to the behavior in Example 3, the spike centered at $x = 0$ that has the smallest height, collapses on an $O(1)$ time scale. The other two spikes, which were initially centered at $x_3 = -x_1 = -1/2$, remain virtually stationary for all τ as their locations are consistent with a two-spike symmetric equilibrium solution.

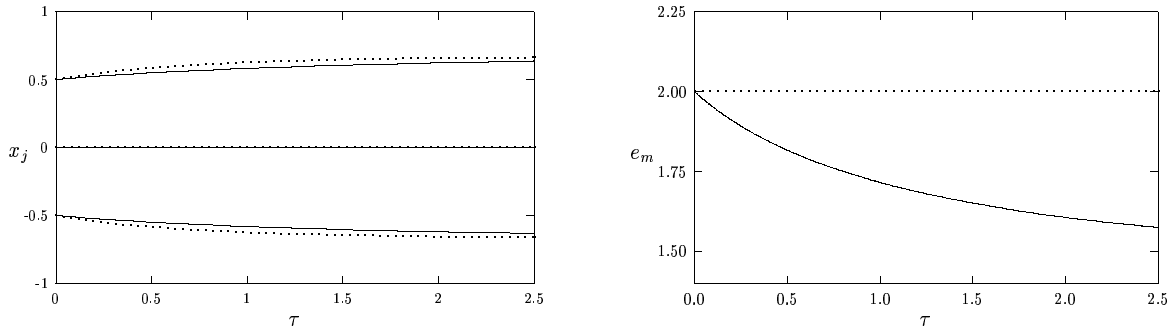

(a) x_j versus τ

(b) e_m versus τ

Figure 9: In Fig. 9(a) we plot x_j versus τ for Example 5. The solid curve corresponds to the full numerical results and the dotted curves corresponds to the asymptotic results. In Fig. 9(b), we plot the maximum eigenvalue e_m of (4.18) versus τ.

τ	x_1 (num)	x_2 (num)	x_3 (num)	x_1 (asy)	x_2 (asy)	x_3 (asy)
0.004	-0.50134	0.0	0.50134	-0.50053	0.0	0.50053
0.1	-0.52484	0.0	0.52484	-0.51239	0.0	0.51239
0.2	-0.54443	0.0	0.54443	-0.52340	0.0	0.52340
0.3	-0.56064	0.0	0.56064	-0.53328	0.0	0.53328
0.4	-0.57434	0.0	0.57434	-0.54224	0.0	0.54224
0.5	-0.58615	0.0	0.58615	-0.55041	0.0	0.55041
0.6	-0.59638	0.0	0.59638	-0.55792	0.0	0.55792
0.7	-0.60535	0.0	0.60535	-0.56485	0.0	0.56485

Table 6: The numerical and asymptotic results for x_1, x_2 and x_3 versus τ for Example 5.

Example 6: (Generic Initial data) We now consider an example where the spikes are initially located at arbitrary positions. We take the parameter values

$$x_1(0) = -0.5\,, \qquad x_2(0) = 0.1\,, \qquad x_3(0) = 0.5\,, \qquad D = 0.04\,. \tag{5.9}$$

For these parameters, we calculate from (4.18) that $e_m(0) = 1.6935$. The asymptotic and numerical trajectories for x_j are compared in Fig. 10(a), and in Table 7. As seen in Fig. 10(b), the maximum eigenvalue e_m once again decreases as τ increases. Thus, the profile is stable with respect to the large eigenvalues and no $O(1)$ instability is triggered at later times.

τ	x_1 (num)	x_2 (num)	x_3 (num)	x_1 (asy)	x_2 (asy)	x_3 (asy)
0.004	-0.50186	0.09228	0.40912	-0.50112	0.09354	0.40539
0.3	-0.62535	-0.00145	0.61632	-0.60449	0.00270	0.59417
0.6	-0.66074	-0.00230	0.65767	-0.65005	-0.00103	0.64704
0.9	-0.66631	-0.00143	0.66480	-0.66286	-0.00103	0.66150
1.2	-0.66692	-0.00818	0.66609	-0.66597	-0.00072	0.66520
1.5	-0.66688	-0.00046	0.66642	-0.66665	-0.00047	0.66617
1.8	-0.66680	-0.00026	0.66654	-0.66676	-0.00031	0.66645

Table 7: The numerical and asymptotic results for x_1, x_2 and x_3 versus τ for Example 6.

5.3 Some General Results

In this section we give two general results related to the dynamics of n-spike profiles. Firstly, we note that the simulation in Fig. 8(a) stops just as e_m approaches the critical value. The simulation

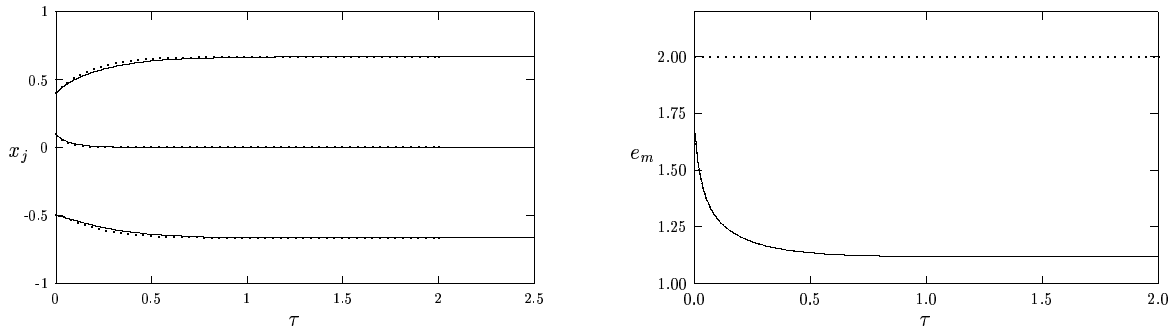

(a) x_j versus τ

(b) e_m versus τ

Figure 10: In Fig. 10(a) we plot x_j versus τ for Example 6. The solid curve corresponds to the full numerical results and the dotted curves corresponds to the asymptotic results. In Fig. 10(b), we plot the maximum eigenvalue e_m of (4.18) versus τ.

stops here not only because the system is no longer valid, but at this value the nonlinear solver for the $\boldsymbol{h}$ system in (2.27) fails to converge. We will demonstrate that when e_m is at the critical value given by the right-hand side of (4.19), the system for $\boldsymbol{h}$ in (2.27) is no longer solvable. Finally we discuss the role of the $O(1)$ eigenvalues on the dynamics of the system.

5.3.1 Solvability of (2.22) at critical values of e_m

The system (2.27) for $\boldsymbol{h}$ is equivalent to that given in (2.22). To show that (2.22) is not solvable at the critical value of e_m, we begin by linearizing this system about

$$\boldsymbol{h} = \bar{\boldsymbol{h}} + \boldsymbol{\theta}\,, \tag{5.10}$$

where $\bar{\boldsymbol{h}}$ is a solution at the critical value of e_m and $\boldsymbol{\theta} \ll \bar{\boldsymbol{h}}$. Substituting into (2.22), we get the linearized problem

$$\left(\mathcal{B} - \frac{b_m(\gamma m - s)}{\sqrt{\mu D}}\mathcal{H}^{\gamma m - s - 1}\right)\boldsymbol{\theta} = 0\,. \tag{5.11}$$

From (4.18) and (4.19) we can see that this equation has a non-trivial solution at exactly the critical value of e_m. This implies that the Jacobian of (2.22) is not invertible at this point. Thus the breakdown, or failure, of the asymptotic ODE system (2.27) occurs exactly at the same point that an $O(1)$ instability is triggered.

5.4 The Collapse Process

From the numerical experiments shown above, and from further numerical computations not shown, we can make some conjectures on the spike collapse process. For an initial n-spike quasi-equilibrium profile, we speculate that when the threshold from (4.19) for an $O(1)$ instability has been exceeded, then at least one of the spikes collapses while the remaining spikes grow. At the end of an $O(1)$ time interval marking the duration of the collapse process, the resulting quasi-equilibrium profile regains its stability with regards to the $O(1)$ eigenvalues, and the remaining spikes will then follow the dynamics of (2.27) until either they reach a stable symmetric equilibrium solution or until another $O(1)$ instability is triggered at a later time, leading to further collapse events. The number of spikes associated with the final equilibrium state depends on the value of D.

A Calculation of the Matrices $\mathcal{B}$ and $\mathcal{PB}$

Consider the boundary value problem

$$Dy'' - \mu y = 0\,, \qquad y'(\pm 1) = 0\,, \tag{A.1a}$$

$$[y]_j = 0\,, \qquad \left[Dy'\right]_j = -\omega_j\,, \tag{A.1b}$$

for $j = 1, \ldots, n$, where $[v]_j \equiv v(x_{j+}) - v(x_{j-})$. The solution is

$$y(x) = \sum_{j=1}^{n} G(x; x_j)\omega_j\,, \tag{A.2}$$

where G satisfies (2.13). Define the n-vectors $\boldsymbol{y}$ and $\langle \boldsymbol{y'} \rangle$ by

$$\boldsymbol{y}^t = (y_1, \ldots, y_n)\,, \qquad \langle \boldsymbol{y'} \rangle^t = \left(\langle y' \rangle_1, \ldots, \langle y' \rangle_n\right)\,, \tag{A.3}$$

where $y_j \equiv y(x_j)$ and $\langle y' \rangle_j \equiv \left(y'(x_{j+}) + y'(x_{j-})\right)/2$. Then, we obtain from (A.2) that

$$\boldsymbol{y} = \mathcal{G}\boldsymbol{\omega}\,, \qquad \langle \boldsymbol{y'} \rangle = \mathcal{P}\boldsymbol{\omega}\,, \qquad \rightarrow \qquad \langle \boldsymbol{y'} \rangle = \mathcal{P}\mathcal{G}^{-1}\boldsymbol{y}\,, \tag{A.4}$$

where $\boldsymbol{\omega}^t = (\omega_1, \ldots, \omega_n)$. Here the matrices $\mathcal{G}$ and $\mathcal{P}$ are defined in (2.23a) and (2.23b), respectively. To determine these matrices explicitly, we solve (A.1) analytically on each subinterval and impose the continuity of y to get

$$y(x) = \begin{cases} y_1 \frac{\cosh[\theta(1+x)]}{\cosh[\theta(1+x_1)]}\,, & -1 < x < x_1\,, \\ y_j \frac{\sinh[\theta(x_{j+1}-x)]}{\sinh[\theta(x_{j+1}-x_j)]} + y_{j+1} \frac{\sinh[\theta(x-x_j)]}{\sinh[\theta(x_{j+1}-x_j)]}\,, & x_j < x < x_{j+1}\,, \quad j = 1, \ldots, n-1\,, \\ y_n \frac{\cosh[\theta(1-x)]}{\cosh[\theta(1-x_n)]}\,, & x_n < x < 1\,, \end{cases} \tag{A.5}$$

where $\theta \equiv \sqrt{\mu/D}$. Imposing the condition $[Dy']_j = -\omega_j$, we can obtain from (A.5) and (A.4) that

$$\mathcal{B}\boldsymbol{y} = \frac{1}{\sqrt{\mu D}}\boldsymbol{\omega}\,, \qquad \rightarrow \qquad \mathcal{G} = \frac{1}{\sqrt{\mu D}}\mathcal{B}^{-1}\,, \tag{A.6}$$

where $\mathcal{B}$ is defined in (2.25). Next, we use (A.4) and (A.6) to get $\langle \boldsymbol{y}' \rangle = \sqrt{\mu D}\mathcal{P}\mathcal{B}\boldsymbol{y}$. By calculating $\langle \boldsymbol{y}' \rangle$ in terms of $\boldsymbol{y}$ from (A.5), we get the formula for $\mathcal{P}\mathcal{B}$ given in (2.26).

Acknowledgements

D. I. thanks NSERC for the support of a graduate student fellowship. M. J. W. would like to thank the support of NSERC grant 81541 and the Mathematics Department of the City University of Hong Kong where most of this paper was written.

References

[1] E. Anderson et al. *Lapack User's Guide: Third Edition*, SIAM Publications (1999).

[2] K. Brenan, S. Campbell, L. Petzold, *Numerical Solution of Initial-Value Problems in Differential Algebraic Equations*, (1989), North Holland.

[3] X. Chen, M. Kowalcyzk, *Dynamics of an Interior Spike in the Gierer-Meinhardt System*, submitted, SIAM. J. Math. Anal., (1999).

[4] A. Doelman, T. J. Kaper, P. Zegeling, *Pattern Formation in the One-Dimensional Gray-Scott Model*, Nonlinearity, **10**, (1997), pp. 523-563.

[5] A. Doelman, R. A. Gardner, T. J. Kaper, *Stability Analysis of Singular Patterns in the 1-D Gray-Scott Model: a Matched Asymptotics Approach*, Physica D, **122**, (1998), pp. 1-36.

[6] A. Gierer, H. Meinhardt, *A Theory of Biological Pattern Formation*, Kybernetik, **12**, (1972), pp. 30–39.

[7] L. Harrison, D. Holloway, *Order and Localization in Reaction-Diffusion Pattern*, Physica A, **222**, (1995), pp. 210-233.

[8] D. Iron, M. J. Ward, J. Wei, *The Stability of Spike Solutions to the One-Dimensional Gierer-Meinhardt Model*, Physica D, **150**, No. 1-2, (2001), pp. 25-62.

[9] D. Iron, M. J. Ward, *A Metastable Spike Solution for a Non-Local Reaction-Diffusion Model*, SIAM J. Appl. Math., Vol. **60**, No. 3, (2000), pp. 778-802.

[10] H. Meinhardt, *Models of Biological Pattern Formation*, Academic Press, London (1982).

[11] NAG Fortran library Mark 17, routine D03PCF, Numerical Algorithms Group Ltd., Oxford, United Kingdom (1995).

[12] D. Morgan, A. Doelman, T. Kaper, *Stationary Periodic Patterns in the 1-D Gray-Scott Model*, Methods and Appl. of Analysis, **7**, No. 1, (2000), pp. 105-150.

[13] C. Muratov, V. Osipov, *Spike Autosolitons in the Gray-Scott Model*, preprint.

[14] W. Ni, *Diffusion, Cross-Diffusion, and their Spike-Layer Steady-States*, Notices of the AMS, Vol. **45**, No. 1, (1998), pp. 9-18.

[15] Y. Nishiura, *Coexistence of Infinitely Many Stable Solutions to Reaction-Diffusion Equations in the Singular Limit*, in Dynamics Reported: Expositions in Dynamical Systems Volume 3 (editors: C. K. R. T. Jones, U. Kirchgraber), Springer-Verlag, New York, (1995).

[16] Y. Nishiura, D. Ueyama, *A Skeleton Structure for Self-Replication Dynamics*, Physica D, **130**, (2000), pp. 73-104.

[17] W. N. Reynolds, J. Pearson, S. Ponce-Dawson, *Self-Replicating Spots in Reaction-Diffusion Systems*, Phys. Rev. E. **56**, (1997), pp. 185-198.

[18] L. F. Shampine, M. K. Gordon, *Computer Solution of Ordinary Differential Equations, the Initial Value Problem*, W. H. Freeman publishers, San Fransisco, (1975).

[19] I. Takagi, *Point-Condensation for a Reaction-Diffusion System*, J. Diff. Eq., **61**, (1986), pp. 208-249.

[20] A. Turing, *The Chemical Basis of Morphogenesis*, Phil. Trans. Roy. Soc. B, **327**, (1952), pp. 37-72.

[21] M. J. Ward, *Exponential Asymptotics and Convection-Diffusion-Reaction Models*, book chapter in *Analyzing Multiscale Phenomena Using Singular Perturbation Methods*, (J. Cronin, R. O'Malley editors), Proceedings of Symposia in Applied Mathematics, Vol. 56, AMS Short Course (1998), pp. 151-184.

[22] M. J. Ward, D. McInerney, P. Houston, D. Gavaghan, P. Maini, *The Dynamics and Pinning of a Spike for a Reaction-Diffusion System*, submitted, SIAM J. Appl. Math., (2000).

[23] M. J. Ward, J. Wei, *Asymmetric Spike Patterns for the One-Dimensional Gierer-Meinhardt Model: Equilibria and Stability*, to appear, Europ. J. Appl. Math., (2001).

[24] J. Wei, *On Single Interior Spike Solutions for the Gierer-Meinhardt System: Uniqueness and Stability Estimates*, Europ. J. Appl. Math., Vol. **10**, No. 4, (1999), pp. 353-378.

[25] J. Wei, *Point–Condensations Generated by the Gierer-Meinhardt System: a Brief Survey*, book chapter in "New Trends in Nonlinear Partial Differential Equations 2000", (Y. Morita, H. Ninomiya, E. Yanagida, and S. Yotsutani editors), pp. 46-59.

[26] J. Wei, M. Winter, *Existence and Stabilty Analysis of Multiple-Peaked Solutions*, preprint, (2001).